Exploration of RF-Controlled High Current Density Hollow Cathode Concepts

Matthew L. Plasek,* Benjamin Jorns,* Edgar Y. Choueiri†

Electric Propulsion and Plasma Dynamics Laboratory

Princeton University, Princeton, NJ 08544 USA

James E. Polk‡

Jet Propulsion Laboratory, California Institute of Technology, M/S 125-109

4800 Oak Grove Drive, Pasadena, CA 91109 USA

Exploration of a novel RF-Controlled Hollow Cathode concept is presented using finite element analysis. Commercial software is used to model the extent of RF power absorption in one configuration of such a cathode in order to describe whether the RF power is localized as in a "stinger" concept or is projected downstream to lower the emission current density while maintaining a constant discharge current. Plasma conductivity along the major axis is calculated from a baseline high current density lanthanum hexaboride hollow cathode and is used in the modeling of RF power absorption by the internal plasma. It was found that within a maximum axial distance from the orifice, a direct coaxial-cathode mating can lead to high percentages (>96%) of localized microwave power absorption. The configuration analyzed acted more as a stinger, as approximately 62% of the RF power was absorbed within 2 mm of the inner coaxial conductor tip. Xenon gas breakdown using RF waves was explored and deemed practical for the cathode parameters studied. RF heating of the emitter prior to plasma ignition was also examined, but low RF power absorption (<5%) without a lossy plasma suggested poor feasibility of this potential function.

Nomenclature

A	thermionic emission equation coefficient
c_0	speed of light
D_0	experimentally modified value of A
e	electron charge
E	electric field
E_c	computed electric field
E_1	electric field at port 1, upstream
E_2	electric field at port 2, downstream
$f_{\text{co,coax}}$	cutoff frequency for a coaxial waveguide
$f_{\text{co,wg}}$	cutoff frequency for a cylindrical waveguide
f_{source}	frequency of a RF source
H	magnetic field
J	thermionic emission current density
k	Boltzmann's constant
k_0	wave number
n	outward normal vector
P_{a}	power absorbed by a lossy medium

*Graduate Research Assistant, EPPDyL; Mechanical and Aerospace Engineering Dept., Student Member AIAA.

†Chief Scientist, EPPDyL; Professor, Applied Physics Group, Mechanical and Aerospace Engineering Dept.; Fellow AIAA.

‡Principle Engineer, Propulsion and Materials Engineering Section, Associate Fellow AIAA

P_{in}	power incident on a port
$P_{\text{r},1}$	power reflected at port 1, upstream
$P_{\text{r},2}$	power reflected at port 2, downstream
r_t	spatial coordinates
S_{ij}	scattering parameter
S_{11}	scattering parameter, reflection coefficient
S_{21}	scattering parameter, transmission coefficient
T	thermionic insert temperature
α	temperature coefficient of the material work function
β	wave propagation constant
δ_z	wave damping in propagation direction
Δ_{dB}	attenuation of a propagating wave
ϵ_0	vacuum permittivity
ϵ_r	relative permittivity
μ_0	vacuum permeability
μ_r	relative permeability
ϕ_0	temperature independent work function
ϕ_{wf}	material work function
ω	wave frequency

I. Introduction

State of the art hollow cathodes have met most solar electric propulsion and commercial lifetime requirements through extended life tests that have proven 28,000 hours (28 kh) of operational life and longer.[1–4] However, previously proposed nuclear electric propulsion missions[3,5] require lifetimes up to 100 kh. In addition to extended lifetimes, recent trends in space power generation are expected to make an order of magnitude higher power levels available for propulsion.[6] The U.S. Air Force Research Laboratory (AFRL) projects that electric thrusters will need to be capable of processing 100-200 kW of power in the near- to mid-term, dwarfing the 0.5 to 12 kW range of recent focus.[7] At the moderate specific impulse of AFRL interest (between 2000-6000 seconds), this translates to roughly 330-660 A of discharge current, 1-2 orders of magnitude higher than currents commonly used in electric thrusters today (e.g. the nominal 20 A for a 6 kW laboratory Hall thruster).[8]

Progress has recently been made on this front as Goebel and Chu[9] experimentally showed that lanathanum hexaboride (LaB_6) bulk-emitting hollow cathodes can successfully achieve up to 250 A of discharge current with an expected life of 10-20 kh. Van Noord, et al.[10] describe the design and testing of a dispenser cathode at 50 A with a predicted life of 100 kh. Even with these advances, we can conclude that large enough improvements are needed in the mid-term to warrant pursuit of novel cathode concepts that could meet these goals.

For hollow cathodes, a sharp peak in plasma density corresponds to a small plasma attachment area, or plasma-emitter contact area, and therefore high current densities and high temperatures result, as reported in many studies.[11–14] The life of a hollow cathode can be estimated to a first order based on the evaporation rate of the emitter material which varies with the current density.[4,9,15,16] Therefore, by increasing the plasma attachment area and lowering the current density peak, we expect the resulting lower temperature to increase the lifetime of the emitter and cathode.[8]

Extending cathode lifetime therefore requires lowering the current density while maintaining the same discharge current. Meeting this goal would also allow the alternative of fixing the current density at the cathode's material thermal limit and sustaining much higher discharge currents while maintaining the same lifetime. A third option is to choose some balance between increasing lifetime and the discharge current.

This paper explores a novel concept that, depending on power absorption, will behave between two identified possibilities. In the configuration analyzed, the RF absorption could occur in a small volume relative to the cathode cavity, acting as a "stinger," where absorption occurs near a conducting rod or probe-like device. Another possibility is that the configuration could project substantial RF power downstream and allow control of the plasma attachment area to lower the current density while maintaining the same discharge current.

We start in Section II, with a description of the new concept and a discussion of some of the design trade-offs with respect to different possible configurations and related solutions that can give the electric propulsion engineer more design space to optimize for specific thruster requirements. We then present in Section III a numerical exploration of RF power absorption in such a cathode concept, using the COMSOL Multiphysics® software package. We use the insight gained to evaluate one configuration's potential for significant RF absorption and the distance over which the absorption takes place. We also evaluate the potential for RF breakdown at cathode emission startup and RF heating of the cathode prior to plasma ignition.

II. Exploration of the Radio Frequency-Controlled Hollow Cathode

A. Selection of a Baseline Hollow Cathode

We select a baseline hollow cathode design that has shown potential to reach high currents and long lifetimes. We will use this baseline as a basis for our calculations as well as a benchmark in future work. To select a baseline cathode type, a succinct review is useful to understand how emitters work, what types are available, and how geometry affects our goals.

1. Thermionic Electron Emitter Physics

Hollow cathodes provide electrons via thermionic emission for which the current density is given by the Richardson-Dushman Equation:[16]

$$J = AT^2 \exp\left(\frac{-e\phi_{\mathrm{wf}}}{kT}\right). \tag{1}$$

Due to significant experimental variations from the theoretical constant A=120 A/cm^2·K^2, an experimentally found temperature dependence (Eq. 2) can be substituted into the Richardson-Dushman equation (Eq. 1) to form the modified current density equation (Eq. 3) where D_0 is material-specific.[16]

$$\phi_{\mathrm{wf}} = \phi_0 + \alpha T, \tag{2}$$

$$J = A \exp\left(\frac{-e\alpha}{k}\right) T^2 \exp\left(\frac{-e\phi_0}{kT}\right) = D_0 T^2 \exp\left(\frac{-e\phi_0}{kT}\right). \tag{3}$$

A hollow cathode insert emits electrons via thermionic emission under the effect of an electric field. This electric field is generated by the internal plasma sheath and the external positively-biased cathode keeper. Plasma outside the cathode also affects the electric field since the external plasma potential is higher than the internal plasma potential.[14] The applied electric field effectively lowers the material work function that emitted electrons must overcome as first described by Schottky.[17] The addition of the Schottky effect or field-enhanced thermionic emission can be incorporated into Eq. 3, resulting in Eq. 4:

$$J = D_0 T^2 \exp\left(\frac{-e\phi_0}{kT}\right) \exp\left(\frac{-e}{kT}\sqrt{\frac{eE}{4\pi\varepsilon_0}}\right). \tag{4}$$

A hollow cathode uses an insert of a specific material composition to act as a low-work function emitter in order to achieve the lowest temperature possible for a given current density (as seen from Eq. 4). The internal plasma density is generally high enough to prevent space-charge limitation and the current density is instead thermally limited by cathode materials.[14]

2. Selection of an Emitter Insert Composition

High current density hollow cathodes can be broadly separated into two types: dispenser and bulk emitter cathodes.[14] Of dispenser cathodes, the most common "Type S" is composed of barium calcium aluminate impregnated into a porous tungsten matrix with a work function of 2.06 eV.[14] These barium-oxide dispenser cathodes sometimes contain other refractory metals to further reduce the work function ("mixed metal matrix" cathodes).[14] Adding scandium to produce a scandate-barium oxide-tungsten emitter results in even lower work functions as small as 1.7 eV.[14] Dispenser cathodes require chemical reactions to enable a low work function. This dependence means dispenser cathodes are easily poisoned by impurities such as oxygen and

water in the propellant or the environment that can drastically raise the effective work function.[14] Despite this drawback, dispenser cathodes have lower work functions than bulk emitters and thus require lower temperatures to sustain a given current density.[14]

Due to these low work functions, dispenser cathodes have been the primary emitter of choice for ion thrusters manufactured in the U.S.[18] In contrast, Russian-made SPT Hall thrusters have used lanathanum hexaboride (LaB_6) bulk emitter cathodes, with hundreds flown since 1971.[9] The first U.S. reported use of LaB_6 for hollow cathodes was by Goebel, et al.,[14] in 1978. More recently, NASA's Jet Propulsion Laboratory has developed high current LaB_6 cathodes for high power Hall thrusters.[9,14] Since 2004 LaB_6 cathodes have also seen commercial use by U.S. based Space Systems/Loral© in SPT-100 Hall thrusters.[19]

The use of LaB_6 bulk emitter has spread to the U.S. due to the emitter's ability to strongly resist poisoning in comparison to dispenser cathodes, despite the higher 2.67 eV work function of polycrystalline LaB_6.[14] LaB_6 is the emitter material itself and does not require any chemical reactions to maintain its low work function. LaB_6 also resists other forms of failure affecting dispenser cathodes.[14] In spite of the higher temperatures required of LaB_6 to achieve the same current density as a dispenser cathode, simulations using lifetime models have shown that LaB_6 actually achieves a longer life due to a lower evaporation rate below around 15 A/cm^2 and more bulk emitting material available for the same size as compared to dispenser cathodes.[9,16] For comparison, tungsten has an order of magnitude higher evaporation rate than both dispenser and bulk emitter cathodes up to current densities of 30 A/cm^2.[16]

Due to strong resistance to poisoning, longer simulated life, and demonstrated ability to reach high current densities above 20 A/cm^2 (at $\sim$ 1700°C) and high currents up to 250 A,[9] we have chosen LaB_6 as the emitter for our cathode concept.

3. Selection of Baseline Geometry

We are interested in achieving high discharge currents with long lifetimes. The LaB_6 cathodes designed and tested by Goebel and Chu[9] were built for high current and tested up to 250 A. The 1.5 cm diameter cathode as described in Ref. 9 will be our starting point. The selected cathode is a trade-off between reaching high currents and keeping the cathode size constrained. It has a predicted life of 12 kh at 100 A of discharge current, and although the predicted life is much below our goal of 100 kh, Goebel and Chu[9] report that simply elongating the emitter insert can increase life in this geometry since significant plasma density was found to extend beyond the emitter in their tests.

If we double the length of the emitter to 5 cm while keeping the cathode geometry constant, and specify the LaB_6 current density to be about 20 A/cm^2 at 1700°C, as per Ref. 9, then the maximum discharge current also doubles to 200 A. At twice the length it can be assumed, from the plasma densities reported in Ref. 9, that at 200 A some upstream part of the insert will be space-charge limited due to a drop-off in plasma density. A concept that causes power to be absorbed in this upstream insert region is expected to increase plasma density and prevent space-charge limitation. The RF-Controlled Hollow Cathode (RF-CHC) concept introduces an RF discharge which has the potential to project power into the desired insert region with significant absorption.

B. Conceptual Design

One possible benefit of the RF-CHC is a lower current density while maintaining the same discharge current. We hypothesize that by adding energy via RF waves at a specific location, the axial plasma density profile and corresponding plasma attachment area can be controlled. If the RF power absorption occurs over a significant distance (on the order of centimeters), the absorption could broaden the plasma attachment area and increase the corresponding flattening of the plasma density profile by adding energy to produce a similar plasma upstream, shown schematically in Figure 1. For cathodes operating in a regime where the plasma density falls off and emission becomes space-charge limited at some upstream location along the emitter insert, broadening the plasma attachment will enlarge the emission area and thus reduce current density at a constant discharge current.[8] If the power absorption is found to occur over shorter distances (on the order of millimeters), the RF-CHC could instead be used as a stinger to provide localized, relatively dense plasmas in regions of interest.

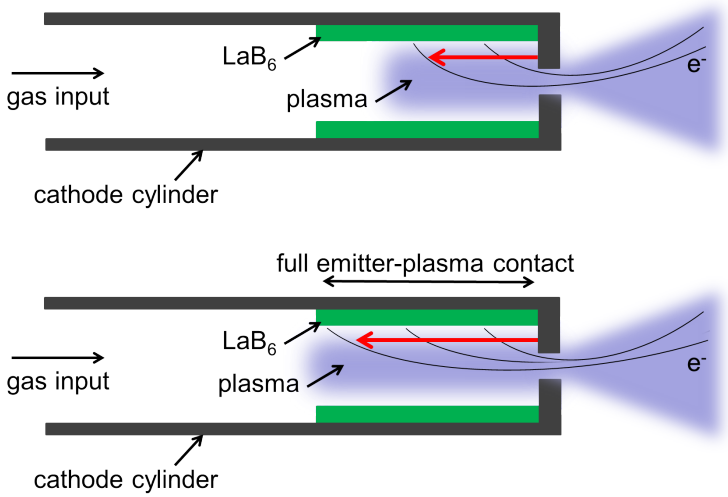

Figure 1. Side views of a basic cathode schematic showing limited plasma attachment area, or reduced plasma-emitter contact area, along the length of the emitter (top) compared to plasma attachment to the full emitter area (bottom). Plasma attached to the entire insert area allows electron emission along the complete length of the emitter.

1. Two-Stage Configuration

One implementation of the RF-CHC concept relies on adding an RF energy pre-stage to the standard LaB_6 cathode, shown in Figure 2. An RF antenna would be embedded in, or encircle, a pre-stage section made of a dielectric, like ceramic. A pre-stage with a dielectric wall would allow the RF waves to pass through ceramic cylinder while maintaining a high temperature barrier between the internal plasma and the antenna. Refractory metals or graphite are commonly used[14] for the cathode cylinder and are opaque to electromagnetic waves due to their significant electrical conductivity. RF energy would be added in the pre-stage immediately upstream of the second stage emitter insert as shown schematically in Figure 2.

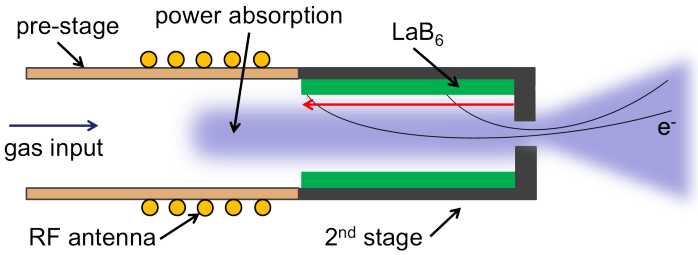

Figure 2. Two-stage configuration of the RF-CHC LaB_6 hollow cathode with the dielectric pre-stage on the left, encircled by a RF antenna. RF power is deposited near the upstream insert region, inside the pre-stage.

2. Single-Stage Configuration

Another configuration of the RF-CHC, depicted in Figure 3, is a single-stage device where RF waves of higher frequencies (1-40 GHz range), or microwaves, are injected upstream of the cathode and intended to propagate downstream, along the cathode major axis to the plasma attachment region. This configuration mates the upstream end of the cathode to a microwave source via a waveguide and effectively treats the conductive cathode cylinder as a cylindrical waveguide. Gas enters the cathode after a dielectric gas break in the waveguide which prevents back flow.

A waveguide mating can be used if the microwave frequency is above the cylindrical waveguide cutoff frequency ($f_{\mathrm{co,wg}} \approx 12$ GHz for our baseline cathode geometry). A cylindrical wave guide allows prediction

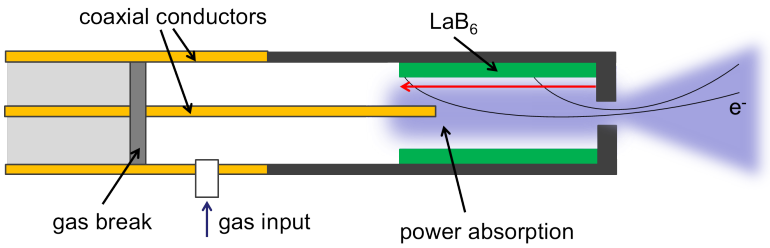

Figure 3. Single-stage configurartion of the RF-CHC LaB_6 hollow cathode with the upstream end on the left, mated with a coaxial cable. RF power arrives from the left where power is deposited in the plasma near the upstream insert end. This configuration was selected for analysis.

of the location of greatest magnitude electric field from a Tranverse Electric (TE) or Tranverse Magnetic (TM) wave mode and can be impedance matched with common tuning mechanisms (e.g. a triple stub tuner).[20,21] Electron Cyclotron Resonance (ECR) heating was considered but the high frequency required to meet the TE_{11} mode cutoff in the baseline cathode geometry also requires a magnetic field approaching 0.5 T for resonance. This magnetic field strength is well above common magnetic fields used in ECR and is difficult to reach with the thermal characteristics of the system (e.g. Curie temperature of permanent magnets). For our analysis, we are interested in the location of strongest electric field as this is where most of the RF energy is expected to be absorbed by the plasma through heating, and where breakdown would occur if RF is used as an ignition source.[20]

If a lower frequency source is preferred due to expense or availability, it is possible to use a coaxial cable mating to propagate a Transverse ElectroMagnetic (TEM) wave into the cathode cylinder. A wave frequency below $f_{co,wg}$ will not propagate in the cathode once two conductors are no longer present (where the inner conductor ends), but this configuration will still allow the energy to be absorbed into the cathode plasma at low microwave frequencies (see §III.B). A coaxial cable can also be used at wave frequencies higher than $f_{co,wg}$ for a flexible connection between the source and cathode. Staying below the coaxial cutoff frequency ($f_{co,coax} \approx 7.5$ GHz for the baseline) allows only a TEM mode to propagate without interference from TE or TM modes. Coaxial cable dimensions can be selected to carry a microwave source frequency, f_{source}, able to meet the needs of a given microwave source and desired cathode mating.[20] In order to propagate a TEM wave mode with minimal interference in a coaxial line and transition into propagating a TE or TM mode in a cylindrical cathode waveguide, it is required that:

$$f_{co,wg} < f_{source} < f_{co,coax}. \tag{5}$$

Ideally, we want the microwave energy to be so fully absorbed in the emitter region as to produce no reflections. To achieve this, the cathode must be seen as a dummy load by the incident microwaves. A dummy load would be perfectly impedance matched and would absorb all of the transmitted wave power from the microwave source. In practice, impedance matching is difficult with an impedance-varying plasma.[21]

We also note that a microwave source requires a potentially life-limiting cathode for electron emission. Various space-qualified microwave sources (e.g. Traveling Wave Tube Amplifiers or TWTAs) use cathodes that have lifetimes which extend beyond the stated hollow cathode lifetime goal of 100 kh as tested by Windes, et al.[22] The cathodes with lifetimes >100 kh are usually mixed metal matrix cathodes and can achieve such lifetimes due to relatively low operating temperatures (<1000°C) and low current densities (1-2 A/cm^2).[22]

C. Comparison of Configurations

While at this conceptual stage of development RF power efficiency is not a primary concern, a high enough percentage of power needs to be absorbed by the plasma in order to warrant the additional system complexity of an RF source. A challenge of the two-stage configuration is ensuring that enough power from the RF antenna is transferred to the cathode without requiring an unreasonable amount of antenna input power. The mismatch between the characteristic RF antenna wavelength, which is on the order of 10 m for a source frequency in the MHz range, and the dimensions of the pre-stage cylinder (around 1-10 cm) would lead to low energy coupling.[20]

Another related challenge is material thermal limitations. An embedded antenna would give the greatest amount of radiated power to the pre-stage as the distance between the pre-stage and the antenna is minimized. However, if the antenna is in thermal contact with the pre-stage, high temperature and a resulting high impedance should be expected. In contrast, the antenna could be thermally isolated and actively cooled. Thermal isolation and cooling would allow for greater antenna input power, but at the cost of increased distance from the target which would lower the amount of radiated power available to the pre-stage. As a thermal advantage, a dielectric pre-stage would likely be less thermally conductive than the typical refractory metal or graphite, and would allow for less heat loss and a decreased heater power level to reach startup temperature.

The single-stage configuration solves the challenges related to having the RF waves introduced from outside of the cathode by directly mating a waveguide or coaxial cable from a microwave source to the upstream end of the cathode cylinder. This results in a minimal loss of wave energy before the high-frequency RF waves (microwaves) are introduced into the cathode. However, the single-stage comes with its own set of complexities. The mating of the cathode and waveguide/coaxial cable requires matching diameters and materials in such a way as to minimize impedance mismatches. A DC break must be incorporated into the inner conductor of the coaxial line to separate RF and DC circuits since the cathode will be kept at a negative bias. A gas break that can manage plasma contact and is transparent to microwaves (e.g. alumina) must be fitted into the waveguide/coaxial cable at an appropriate depth.

Sputtering of the inner and outer conductors of the coaxial line, or of the waveguide after the gas break, may need to be addressed. At microwave frequencies (1-40 GHz) the ions are too massive to have much response in the short time scale before the electric field switches orientation, so even for coaxial potential differences in the hundreds of volts, significant ion sputtering of the antenna is not expected. Also, LaB_6 cathodes, like our baseline cathode, have insignificant internal sputtering from low energy ions due to an internal plasma potential less than 15 V.[9] If appreciable erosion does occur, the conductors of the waveguide or coaxial cable could be insulated with a ceramic, like alumina, which is a common insulation for RF antennas that are exposed to ion sputtering.[14]

The single-stage configuration has more geometrical parameters to consider that affect energy transmission than the two-stage configuration. The conceptual design space is still large and geometric parameters are related to all aspects of RF-CHC performance. The basic concept of the single-stage configuration has the advantage of minimal input-power loss compared to the two-stage configuration. In addition, a coaxial mating gives the most flexible parameter space for experimental purposes and as such, we chose the coaxial single-stage RF-CHC configuration to be the focus of our analysis and discussion. We assumed a relatively inexpensive and common 2.45 GHz microwave frequency.

D. Comparison to Recent Developments in the Literature

1. Methods to Increase Life and Discharge Current

There has been significant effort, documented in recent literature, for improving life and maximum discharge current in hollow cathodes. We present here an overview of these efforts and their relevance to the RF-CHC concept.

In 2006, Van Noord, et al.[10] discussed the results of increasing the thickness of the hollow cathode walls in the emitter region in order to increase thermal conduction and decrease the temperature variation. Less temperature variation along the emitter insert leads to a more uniform emission and plasma density profile. Although increasing the thermal conduction along the emitter region showed improvement in attachment area,[10] generally thinner walls and longer cathodes having minimal conduction upstream of the emitter are desired for lower heater power.[9, 23]

A second method to lower current density and increase the maximum current was proposed by Van Noord, et al.,[10] and relies on increasing the emission area by increasing the insert diameter. A cathode designed following these methods reached a predicted lifetime of 100 kh at 50 A of discharge current.[10] Goebel, Watkins, and Jameson[16] showed in 2007 that, generally, hollow cathodes of larger sizes can achieve longer lifetimes. The authors compared three different sizes of LaB_6 hollow cathodes (0.8, 1.5, and 2.0 cm diameters) and predicted a lifetime of 100 kh at 75 A for their 2.0 cm diameter cathode.

In 2010, Goebel and Watkins[23] found that as the orifice diameter is increased the area of the plasma attachment increases and the axial plasma density profile broadens. The authors[23] noted that increasing discharge current and mass flow rate will push the peak plasma density towards the orifice. In a small-

diameter orifice cathode, pushing the plasma density peak toward the orifice leads to a narrowing of the plasma density profile and decreased plasma attachment to the emitter. In comparison, plasma attachment to the full emitter area was maintained by the large-diameter orifice cathode tested in Ref. 23. Predicted lifetime of the large-diameter orifice cathode was 100 kh at 20 A of discharge current or 10 kh at 45 A.[23]

Goebel and Watkins[23] also noted that an increase in LaB_6 insert thickness could lead to a longer lifetime with lifetime estimated from emitter evaporation rate. We note that both the beginning-of-life and the predicted end-of-life insert inner-diameters must be considered when selecting an insert thickness. Insert thickness is a trade-off between cathode lifetime limited by emitter evaporation and the emitter area available to reach a desired discharge current.

In 2011, Goebel and Chu[9] developed and tested high current LaB_6 cathodes having 1.5 and 2.0 cm diameters and lengths between 6 and 15 cm, depending on the application. In their case, the orifice was sized to 80% of the inner insert diameter and significant plasma density extended beyond the insert.[9] Hence, increasing the length of the insert would decrease current density and increase life. For even longer lifetimes, Goebel and Chu[9] suggested a larger cathode diameter as proposed previously.[10] The 1.5 cm diameter cathode from Ref. 9 had a predicted lifetime of 12 kh at 100 A discharge current, whereas the 2.0 cm cathode's lifetime was predicted to be 20 kh at 200 A.[9]

The same authors[9,10,16,23] suggested increasing various dimensions of the hollow cathode to achieve lower current densities at a given discharge current. To raise the maximum discharge current, the insert dimensions must increase to provide a larger emission area. Increasing cathode and insert size can be difficult for geometry-constrained thrusters. An example of a geometry-constrained application is the internally-mounted cathode for Hall thrusters. The internally-mounted cathode has been shown to increase total Hall thruster efficiency, lower thruster plume divergence and increase plume symmetry.[5,24] Although thrusters are expected to scale in size with increased power, there are also expected to be geometry-constrained applications in the near- to mid-term, such as internally-mounted cathodes for high power Hall thrusters or for concentric channel Hall thrusters that have gained significant interest from the Air Force.[7,25]

Since an internally-mounted cathode is located in the center of a Hall thruster annulus, the cathode length is the only relatively unconstrained dimension. Assuming the baseline cathode outside-diameter of 1.5 cm and a large-diameter orifice to increase the plasma attachment area, a long insert (5-10 cm) required for high discharge current ($\geq$ 200 A) is expected to be space-charge limited at some upstream location as with our previous example in §II.A.3. Controllable RF power absorption near the upstream emitter region would increase plasma density so that no part of the longer insert is space-charge limited.

2. Relevance to Plume Mode

With an increased cathode orifice diameter, the neutral pressure is lower and the axial internal plasma density profile benefits by becoming broader and more uniform. However, the combination of a low cathode gas flow rate and a large-diameter orifice can reduce the cathode neutral pressure enough to induce a transition from "spot" mode to "plume" mode.[14] Plume mode is cited as the likely cause of plasma oscillations and the production of energetic ions that can seriously erode the cathode keeper end plate and cathode, causing off-design operation and eventual failure.[26–30] Quenching plume mode is often achieved by reducing the discharge current, increasing the mass flow rate, or decreasing the diameter of the orifice.[26,29] These are all undesirable solutions in our case, as we want to increase, not decrease, the discharge current, and the latter two solutions of increasing mass flow rate and decreasing the orifice diameter push the plasma density peak towards the orifice, decreasing the plasma attachment area. Goebel, et al.,[29] also noted that judicious use of materials with low sputtering yields can help mitigate the problems associated with plume mode and high-energy ion bombardment.

Goebel, et al.,[26,27] introduced a method for quenching the plume mode by injecting cold gas into the cathode plume immediately outside of the cathode assembly. The external gas injection allows the internal cathode mass flow rate to drop significantly, leading to a 50% reduction in the total thruster gas consumption.[26,27] Since the cathode gas flow rate is decreased, the internal neutral pressure is lower and the plasma attachment is broader, as described before. Also, as noted in Ref. 26, lower current densities tend to reduce the high-energy ion production and plume mode oscillations. The ability to project RF power into the insert region downstream could be used in addition to external gas injection to increase the plasma attachment area.

Earlier in 2012, Goebel, et al.,[8] showed that the gas flow fraction for the cathode (typically 7-10% of the total thruster gas flow rate), can be reduced to lower levels (5% or lower) without entering the plume mode.

Again, this lower cathode gas flow rate resulted in plasma attachment broadening. The authors showed[8] that without this broadening, a drop-off in plasma density can cause the electron emission along the insert to become space-charge limited at some distance from the orifice. For example, if the insert length is increased and the mass flow rate is decreased as suggested, the plume mode could be avoided while the predicted life was increased by four times.[8]

As per the reviewed literature, a lower cathode gas flow rate and a larger-diameter orifice increases plasma attachment area but can lead to the plume mode. With a concept that projects RF power downstream, we can increase the plasma attachment area beyond the initial broadened attachment accomplished by an appropriate gas flow rate and orifice size to keep a minimum neutral pressure in order avoid the plume mode. Depending on configuration and design parameters to be explored, the RF-CHC concept holds the potential to project RF power downstream.

III. Analysis and Results

A. Modeling

We selected the coaxial line single-stage configuration (from §II.C) as the focus of our analysis. To explore the potential of the RF-CHC concept to input RF power into the internal cathode plasma at a specific location, we numerically modeled a set of partial differential equations (PDEs) for electromagnetic wave propagation in three dimensions using COMSOL Multiphysics® v3.5a. The COMSOL® RF Module was used to perform three-dimensional finite element analysis of a TEM wave mode propagating in coaxial cable, incident on the upstream end of the cathode. Relevant input parameters and boundary conditions are summarized below. Our solutions were found to be independent of further mesh refinement, with mesh element sizes several times smaller giving less than 0.1% change in power absorption and electric field strengths appearing the same throughout. Further details of the numerical modeling can be found in the Appendix.

As seen in Figure 4, we created a 3D model of a segment of the baseline hollow cathode with a coaxial cable mated to the left, upstream end. In the geometry modeled, the inner coaxial conductor ends before the insert region farther downstream, however, the inner conductor could be designed to extend far into the insert region if desired. The inner cavity was split into four separate, solid volumes and assigned different conductivities to approximate a plasma conductivity profile along the length of the cathode. More simplistic single-volume and two-volume conductivity geometries were modeled as well. However, we found the accuracy of the RF power absorption modeling to be higher with more volumes. A four-volume geometry was found to capture the essential behavior of the RF power absorption. We calculated the plasma conductivities from baseline cathode parameters and relevant formulas from Goebel and Chu,[9] Mikellides, et al.[12] and others.[14, 20]

We used classic resistivity based on electron-neutral and electron-ion collisions to calculate a first-order approximation of the plasma conductivity profile. Although, according to Mikellides, et al.,[12] anomalous resistivity is expected to exist due to micro-instabilities. We assume any anomalous resistivity is negligible in this preliminary analysis. Calculations of the plasma parameters were verified by comparing them to the results in Ref. 12.

The internal cavity was split into four discrete volumes, as shown in Figure 5, and each has a different calculated plasma conductivity which progresses from lower to higher conductivity starting from the left, upstream end with Volume 1: 0.08, 0.4, 3.7, and 300 S/m. These conductivities qualitatively match the results from Ref. 9. Our region of interest is farther upstream than most authors have focused on as we are interested in where the plasma density falls off to space-charge limited levels.

The models' solutions yielded the electric field magnitude and scattering parameters, S_{ij}, which were converted into the absorbed and reflected RF power. The RF waves were perfectly matched at the incident boundary and no reflections occurred at the upstream or downstream end boundaries. At the incident upstream boundary we specified, for all model runs except as noted, the RF power to be 100 W and the microwave frequency to be the relatively common value of 2.45 GHz.

Lossy impedance boundary conditions were modeled by the appropriate materials and their respective approximate conductivities are listed in Table 1. Graphite was modeled for the cathode cylinder walls, copper for the inner coaxial conductor, and LaB_6 for the insert. Depending on design, tungsten or a similar refractory metal could be modeled for the cathode walls or for the inner conductor and is shown in Table 1 for comparison. We found that modeling a tungsten versus a copper conductivity for the inner conductor boundary results in an absorbed power difference of less than 3%.

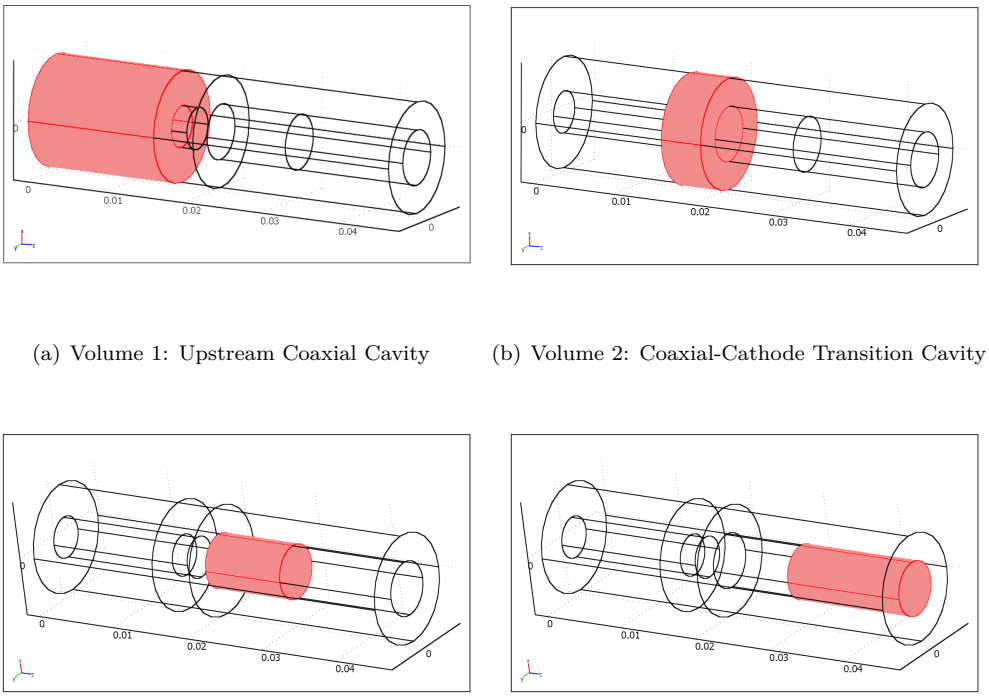

(a) Volume 1: Upstream Coaxial Cavity

(b) Volume 2: Coaxial-Cathode Transition Cavity

(c) Volume 3: Upstream Insert Cavity

(d) Volume 4: Downstream Insert Cavity

Figure 4. 3D views of the hollow cathode inner cavity split into four highlighted volumes for modeling. Each volume was assigned a different plasma conductivity to approximate a plasma conductivity profile. The left is the upstream side with the inner coaxial conductor at the center; the right is the downstream side, surrounded by the insert.

Table 1. Material conductivities used to model boundaries

Material	Conductivity (S/m)
graphite	1.9e4
tungsten	2.1e6
copper	7.9e6
LaB_6	3.0e6

The modeled cathode segment was a section "cut-out" from the coaxial-cathode system. The upstream model end boundary is not located at the gas break, but the two are separated by some axial distance. Similarly, the downstream model end boundary is not necessarily located at the orifice, but the boundary is some distance away from the orifice (approximately 2.5 cm in our baseline case). We were most interested in the coaxial cable-to-cathode transition so, in order to minimize computational cost, only that region was modeled. Due to the relatively high conductivities and plasma densities towards the upstream end of the cathode, the RF waves were either absorbed or reflected, therefore it was not necessary to model the whole system.

B. Results and Discussion

Figures 6 and 7 show a solution to the four-volume stepped conductivity model from which we first note a sudden drop in electric field downstream (Figure 6, Volume 3) and the convoluted electric field streamlines after the inner conductor ends (Figure 7, Volume 4). Here, a streamline is a line, where at any point along the

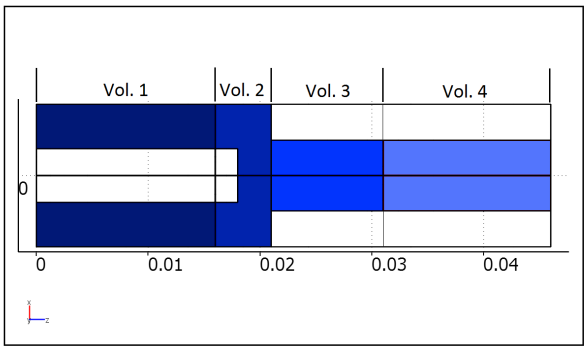

Figure 5. Discrete volumes adopted in the model. The plasma conductivity for each volume starting from upstream with Volume 1: 0.08, 0.4, 3.7, and 300 S/m. The upstream white space to the left is the inner coaxial conductor and the downstream white space to the right is the insert.

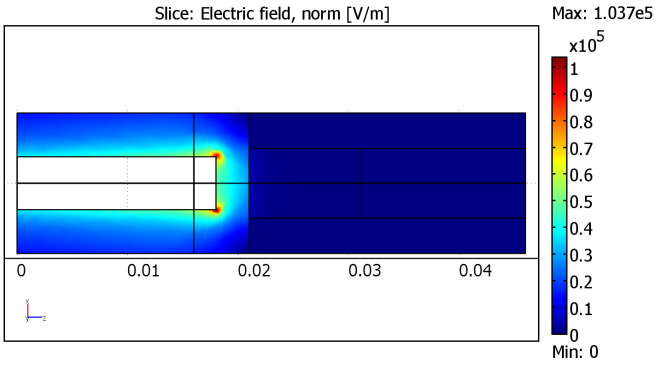

(a) Electric Field Magnitude

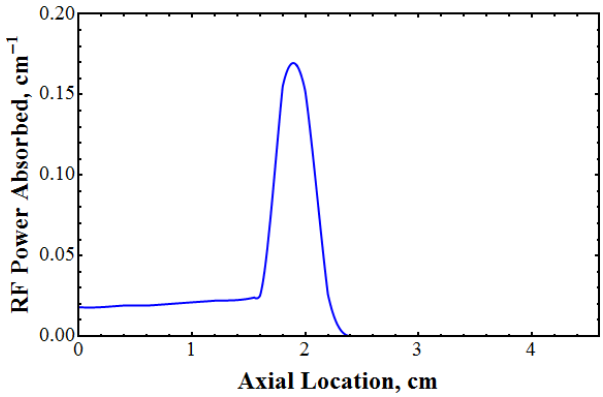

(b) One-Dimensional RF Power Absorption

Figure 6. Calculated electric field magnitude (a) and normalized one-dimensional power absorption (b) for a four-volume model with discrete conductivities. Note the maximum reached at the tip of the inner conductor and the minimum region to the right for both (a) and (b).

line, the electric field vector is tangent to the line. The negligible electric field and non-uniform streamline effects downstream are due the the relatively high plasma conductivity in Volume 4, which is two orders of magnitude above the adjacent Volume 3. At the high level of conductivity in Volume 4, the electric field is negligible and hence the streamlines are indicative of minor fluctuations.

We also note a maximum in the value of the electric field magnitude at the tip of the inner coaxial

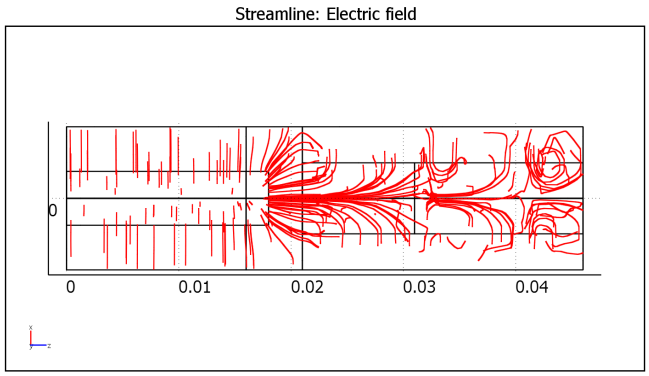

Figure 7. Calculated electric field streamlines for a lossy plasma with stepped conductivities. Note the non-uniform streamlines downstream (right) due to near-zero electric field and transverse electric field upstream (left) due to propagating TEM mode.

conductor (Figure 6, Volume 2). From the dominant electric field in this region, we expect that much of the incident RF power is absorbed in Volume 2. The "port" boundary conditions on both ends of the cathode supply scattering or S_{ij} parameters. In our case, port 1 is the upstream boundary on the left, and port 2 is the downstream boundary. S_{11} is the reflection coefficient whereas S_{21} is the transmission coefficient. COMSOL® defines these S_{ij} parameters in terms of electric field or power flow:

$$S_{11} = \frac{\int_{port1}\left((E_c - E_1)\cdot E_1^*\right)dA_1}{\int_{port1}\left(E_1 - E_1^*\right)dA_1} = \sqrt{\frac{\text{power reflected from port 1}}{\text{power incident on port 1}}}, \tag{6}$$

$$S_{21} = \frac{\int_{port2}\left((E_c - E_2)\cdot E_2^*\right)dA_2}{\int_{port2}\left(E_2 - E_2^*\right)dA_2} = \sqrt{\frac{\text{power delivered to port 2}}{\text{power incident on port 1}}}. \tag{7}$$

In the cases modeled, $S_{21} \approx -\infty$ dB and can be ignored, as this indicates that the power transmitted approaches zero. Therefore, in every case considered, all of the incident RF power (P_{in}) is either absorbed (P_{a}) or reflected (P_{r}). In the solution presented in Figures 6 and 7, $S_{11} = -14.27$ dB. Using the scattering parameters, the power absorbed is given by:

$$S_{11} = 10^{S_{11}/20}, \tag{8}$$

$$P_{\text{r},1} = S_{11}^2 P_{\text{in},1}, \tag{9}$$

$$P_{\text{a}} = P_{\text{r},2} - P_{\text{r},1}. \tag{10}$$

We calculated the absorbed power to be >96% of the incident power. From a one-dimensional power absorption model (Figure 6b), we also found that approximately 62% of this power is absorbed within 2 mm of the inner coaxial conductor tip. This result shows that within a discretized approximation to a plasma conductivity profile, the internal plasma is capable of absorbing high percentages of RF power in a localized, small volume for the single-stage configuration. The power absorption continues upstream from the inner conductor tip region, but since the RF power is not projected downstream, this configuration exhibits the characteristics of a stinger concept where a localized plasma can be created near the inner conductor. Although RF power absorption was not found to occur at a significant downstream distance from the inner conductor tip, it is possible other configurations of the RF-CHC hold that potential and can be used for lowering current density at a constant discharge current.

We note that this near complete localized absorption by the lossy plasma is dependent on the location of the inner coaxial conductor tip and the conductivity profile along the cathode major axis. The region between approximately 2.5 to 7.1 cm upstream of the orifice was selected from the baseline cathode characterization[9] for the cathode segment to model. If we shift the modeled cathode segment upstream or downstream, the conductivity profile changes and a different power absorption results. Therefore, the magnitude of the

localized RF power absorption is partly controlled by the length of the inner coaxial conductor and partly controlled by the neutral pressure given by the cathode gas flow rate and orifice size.

For comparison, Figure 8 shows a solution of a modeled cathode segment with a higher conductivity per volume than those conductivities used in Figure 6. This higher-valued conductivity profile is representative of an effective shift of the cathode segment to approximately 1 cm farther downstream, closer to the orifice (the profile extends from around 1.5 to 6.1 cm upstream from the orifice). The conductivities used, starting from the upstream end with Volume 1, were: 1.0, 2.9, 89, and 1355 S/m.

We note that the maximum of the electric field magnitude has shifted from the inner coaxial conductor tip, as before in Figure 6, to the upstream region of the modeled coaxial segment as per Figure 8. The model shown in Figure 8 has near 100% localized absorption with $S_{11} = -35.12$ dB. As with our previous model, the power absorption is primarily located where the electric field magnitude is the highest, and in this case, the majority of the RF power is absorbed upstream from the conductor tip. The modeled upstream end boundary to the left is somewhat unphysical in this particular case, as RF absorption would likely begin at a lower conductivity located farther upstream before the modeled upstream boundary shown. However, we note that Figure 8 shows the essential effect of a higher-valued conductivity profile on the location of the localized RF power absorption.

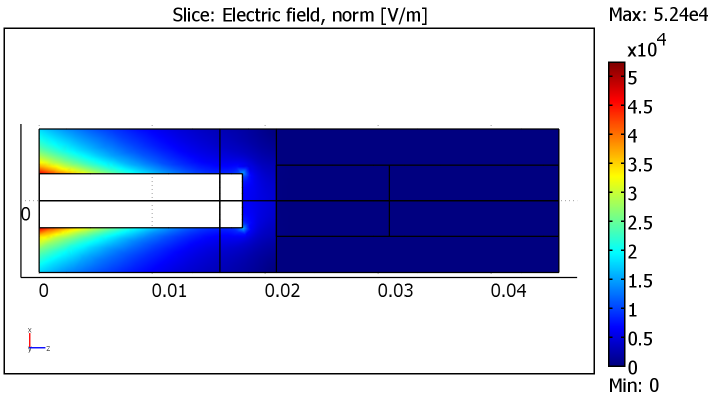

Figure 8. Calculated electric field magnitude for a higher-valued conductivity profile (modeled segment is effectively farther downstream) than the profile used in Figure 6. Note the maximum shifts towards the upstream boundary.

We also considered the possibility of the microwaves acting as the plasma ignition source instead of, or in addition to, the voltage applied to the keeper during emission startup. Figure 9 shows the electric field streamlines solution with the internal cavity as a single, solid volume with negligible conductivity. A neutral gas or a vacuum can be modeled by this negligible-conductivity model. As in our first stepped conductivity model, the electric field magnitude is highest at the tip of the inner coaxial conductor. Streamlines of the electric field are shown in Figure 10. The transverse electric field solutions show that the TEM mode is propagating until the end of the inner coaxial conductor where the electric field streamlines then weaken dramatically and turn axially.

The frequency of the microwaves, the electric field amplitude, and neutral gas pressure determine if breakdown will occur.[31] From previous studies[31,32] and the electric field magnitude shown in Figure 9, we expect that breakdown is achievable well within reasonable power levels (e.g. our assumed microwave incident power of 100 W). The neutral gas pressure of our baseline hollow cathode is well above 1 Torr in the upstream region of interest, which is a greater than the minimum neutral pressure required for neutral xenon gas breakdown at a microwave frequency of 2.45 GHz.[31]

From Table 2 we note that within a range of incident power levels the maximum electric field magnitude stays within the 10^5 V/m order of magnitude. We conclude that a large change in incident microwave power is needed to achieve a maximum electric field magnitude substantially higher than what is achieved with a given initial power. If breakdown is a concern under harsher ignition conditions than those which exist in our baseline hollow cathode, an option would be to provide sharp points in the inner conductor tip geometry which can improve the probability of breakdown due to multiple points of high electric field magnitude, as

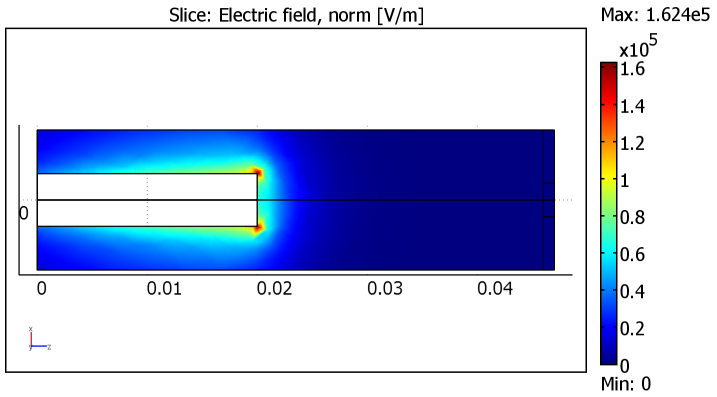

Figure 9. Calculated electric field magnitude for a single, solid volume with negligible conductivity. Note the maximum reached at the tip of the inner conductor, similar to Figure 6.

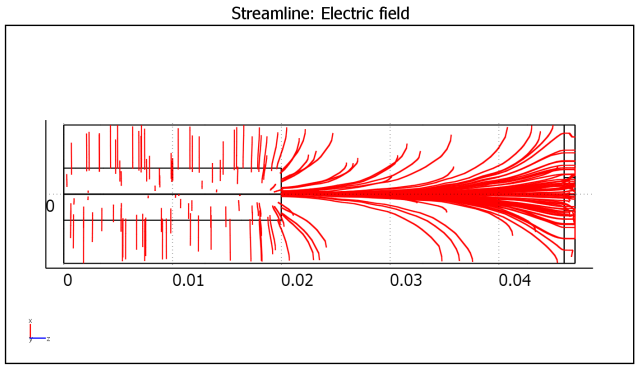

Figure 10. Calculated electric field streamlines for a single, solid volume with negligible conductivity. The electric field streamlines switch from transverse to predominantly axial, similar to a coaxial-waveguide transition.

seen from the corners of the inner conductor in Figure 9.

Finally, we examined heating of the cathode cylinder and insert prior to plasma ignition. Being able to replace the function and power use of the heater with a multi-function RF source is an attractive prospect, although heaters are becoming more reliable under high temperatures, as noted in recent LaB_6 cathode operation.[9]

The solution as seen in Figures 9 and 10 is that for a pre-ignition/pre-plasma model. The S_{ij} parameters and resulting absorbed RF power were calculated as before. Since there is no solid cavity-volume that absorbs the RF power (like our plasma approximation), the absorption is due purely to the attenuation in the walls of the cathode. Lossy boundary conditions were modeled (details in the Appendix) but little overall power was absorbed. The S_{11} parameter for this case was -0.1 dB and the resulting power absorption was 2.6 W, giving an absorption of less than 3% of the incident power.

We find it unlikely that cathode heating prior to plasma ignition could be a viable function for the RF-CHC due to the lack of a lossy, power-absorbing plasma and a low modeled absorption by the cathode materials. We conclude that significant RF power absorption requires a minimal conductivity in the cathode cavity and therefore, during cathode emission, a maximum distance from the orifice exists where the plasma conductivity is too low to significantly absorb RF waves. From our modeling, we expect this distance to be larger than common insert lengths around 2-4 cm.

Table 2. Maximum electric field magnitude vs. incident RF power (negligible-conductivity model)

E (V/m)	Power (W)
1.1e5	50
1.6e5	100
2.3e5	200
2.8e5	300

IV. Conclusion

We explored a novel RF-CHC concept for controlling plasma attachment inside a hollow cathode by adding RF waves to the upstream region of the insert. Specifically, we calculated the plasma conductivity profile and used finite element analysis to show that it is feasible to locally absorb a high percentage of the incident RF power for a coaxial cable mated to a hollow cathode in a single-stage configuration. The single-stage configuration acts as a stinger and provides localized RF power absorption in our analysis. Other RF-CHC configurations may yet hold the potential to project RF power a significant distance downstream. Our modeling suggests that the RF source could break down xenon gas and start cathode emission or play an assisting role to the keeper cathode voltage. Additionally, RF heating of the emitter prior to plasma ignition does not appear likely.

The numerical analysis presented here could be refined in the future, including refinement by use of higher fidelity plasma simulations such as those conducted by Polk, et al., on dispenser cathodes.[33,34] Theoretical modeling and experimental testing is also of interest for future studies. Potential erosion of the inner conductor in the single-stage configuration is of particular interest for future study. As with most new concepts, there is a large parameter space to explore, including cathode and insert geometries, methods of RF coupling with the cathode internal plasma, and axial location of RF input power. A study of a range of RF source frequencies is also warranted for investigating potential RF power projection. In light of these preliminary results, we find that the RF-CHC concept can be a localized source of RF power absorption as modeled, and other RF-CHC configurations to be explored hold the potential to decrease current density at constant discharge current via RF power projection and significant absorption downstream.

Appendix

COMSOL Multiphysics® v3.5a is commercial software package that uses the finite element method to solve partial differential equations (PDEs). The RF Module was used for modeling, and although a Plasma Module exists for COMSOL® v4.3, it was not available for this analysis. Instead, a conductivity profile was calculated and then approximated in the model by applying average conductivity values to the different cavity volumes. A segment of the cathode geometry was modeled in three dimensions and and boundary conditions were applied that captured electromagnetic wave attenuation and power loss.

Our mesh size was found to be acceptable. A mesh refinement study confirmed that only small changes of less than 0.1% in power absorption resulted from refining the mesh multiple times. COMSOL®-supplied solvers were used, and full convergence to the specified tolerance was met on the order of minutes. More detail on the approach can be found in Ref. 35.

The governing PDEs for the 3D electromagnetic waves mode are:

$$\nabla \times (\mu_r^{-1} \nabla \times \mathbf{E}) - k_0^2 \varepsilon_{rc} \mathbf{E} = \mathbf{0}, \tag{11}$$

$$\nabla \times (\varepsilon_{rc}^{-1} \nabla \times \mathbf{H}) - k_0^2 \mu_r \mathbf{H} = \mathbf{0}, \tag{12}$$

where the wave number in free space is defined as:

$$k_0 = \omega \sqrt{\varepsilon_0 \mu_0} = \omega / c_0. \tag{13}$$

Domains that match the impedance of adjacent boundaries (to prevent reflections) and absorb incident RF waves that travel through them are named "Perfect Matching Layers" or PMLs. These domains were used as necessary to absorb reflected power outside the areas of interest in order to ensure that the power

absorption was not due to standing waves. Boundary and interface conditions include those from a "no surface current" condition at the interfaces:

$$\mathbf{n_2} \times (\mathbf{E_1} - \mathbf{E_2}) = \mathbf{0}, \tag{14}$$

$$\mathbf{n_2} \times (\mathbf{H_1} - \mathbf{H_2}) = \mathbf{0}. \tag{15}$$

Although ideal boundary conditions lessen computational expense, the models were manageable enough to include impedance boundary conditions (BCs). These impedance BCs were set to represent specific materials (in our case graphite walls and copper coaxial conductor) that are not perfectly conducting and lead to attenuation of the propagating wave as per the following attenuation and impedance BC:

$$\Delta_{dB} = 20\delta_z \log e, \tag{16}$$

$$\sqrt{\mu_0\mu_r/\varepsilon_c}\mathbf{n} \times \mathbf{H} + \mathbf{E} - (\mathbf{n} \cdot \mathbf{E})\mathbf{n} = (\mathbf{n} \cdot \mathbf{E_s})\mathbf{n} - \mathbf{E_s}. \tag{17}$$

Eq. 17 is used at boundaries where the field only penetrates a short distance beyond the boundary in order to approximate lossy boundaries and save computation cost.

The boundary mode analysis application mode for 3D was used in solving the models. The types of fields that can be described are:

$$\mathbf{H}(x, y, z, t) = \mathbf{H}(\mathbf{r}_t)e^{j(\omega t + \beta(\mathbf{n}\cdot\mathbf{r}))}, \tag{18}$$

$$\mathbf{E}(x, y, z, t) = \mathbf{E}(\mathbf{r}_t)e^{j(\omega t + \beta(\mathbf{n}\cdot\mathbf{r}))}. \tag{19}$$

Acknowledgments

This research has been supported by the U.S. Air Force Office of Scientific Research.

References

[1]Sengupta, A., Brophy, J. R., and Goodfellow, K. D., "Status of the Extended Life Test of the Deep Space 1 Flight Spare Ion Engine after 30,352 Hours of Operation," 39th Joint Propulsion Conference, 2003.

[2]Sengupta, A., "Destructive Physical Analysis of Hollow Cathodes from the Deep Space 1 Flight Spare Ion Engine 30,000 Hr Life Test," 29th International Electric Propulsion Conference, Princeton, New Jersey, 2005.

[3]Goebel, D. M., Katz, I., Polk, J. E., Mikellides, I. G., Jameson, K. K., and Liu, T., "Extending Hollow Cathode Life for Electric Propulsion in Long-Term Missions," AIAA Space 2004 Conference, 2004, pp. 1–12.

[4]Sarver-Verhey, T. R., "Scenario for Hollow Cathode End-of-Life," 26th International Electric Propulsion Conference, Kitakyushu, Japan, 1999, pp. 703–713.

[5]Hofer, R. R., Randolph, T. M., Oh, D. Y., Snyder, J. S., and de Grys, K. H., "Evaluation of a 4.5 kW Commercial Hall Thruster System for NASA Science Missions," 42nd Joint Propulsion Conference, Sacramento, California, 2006.

[6]Capadona, L. A., Woytach, J. M., Kerslake, T. W., Manzella, D. H., Christie, R. J., Hickman, T. A., Scheidegger, R. J., Hoffman, D. J., and Klem, M. D., "Feasibility of Large High-Powered Solar Electric Propulsion Vehicles: Issues and Solutions," AIAA Space 2011 Conference, No. February, Long Beach, California, 2012.

[7]Brown, D. L., Beal, B. E., and Haas, J. M., "Air Force Research Laboratory High Power Electric Propulsion Technology Development," IEEEAC, 2009.

[8]Goebel, D. M., Jameson, K. K., and Hofer, R. R., "Hall Thruster Cathode Flow Impact on Coupling Voltage and Cathode Life," Journal of Propulsion and Power, Vol. 28, No. 2, March 2012, pp. 355–363.

[9]Goebel, D. M. and Chu, E., "High Current Lanthanum Hexaboride Hollow Cathodes for High Power Hall Thrusters," 32nd International Electric Propulsion Conference, Jet Propulsion Laboratory, Wiesbaden, Germany, 2011, pp. 1–16.

[10]Van Noord, J. L., Kamhawi, H., and Mcewen, H. K., "Characterization of a High Current, Long Life Hollow Cathode," 29th International Electric Propulsion Conference, Princeton, New Jersey, 2005, pp. 1–12.

[11]Katz, I., Anderson, J. R., Polk, J. E., and Brophy, J. R., "One-Dimensional Hollow Cathode Model," Journal of Propulsion and Power, Vol. 19, No. 4, 2003, pp. 595–600.

[12]Mikellides, I. G., Katz, I., Goebel, D. M., and Polk, J. E., "Model of a Hollow Cathode Insert Plasma," 40th Joint Propulsion Conference, Fort Lauderdale, Florida, 2004, pp. 1–18.

[13]Katz, I., Mikellides, I. G., Goebel, D. M., and Polk, J. E., "Insert Heating and Ignition in Inert-Gas Hollow Cathodes," IEEE Transactions on Plasma Science, Vol. 36, No. 5, 2008, pp. 2199–2206.

[14]Goebel, D. M. and Katz, I., Fundamentals of Electric Propulsion: Ion and Hall Thrusters, Vol. 1, John Wiley & Sons Inc, 2008.

[15]Kovaleski, S. D., "Life Model of Hollow Cathodes Using a Barium Calcium Aluminate Impregnated Tungsten Emitter," 27th International Electric Propulsion Conference, No. December, NASA, Pasadena, California, 2001.

[16]Goebel, D. M., Watkins, R. M., and Jameson, K. K., "LaB6 Hollow Cathodes for Ion and Hall Thrusters," Journal of Propulsion and Power, Vol. 23, No. 3, May 2007, pp. 552–558.

[17]Schottky, W., "Concerning the Discharge of Electrons from Hot Wires with Delayed Potential," Annalen der Physik, Vol. 44, No. 15, 1914, pp. 1011– 1032.

[18]Goebel, D. M., Polk, J. E., Sandler, I., Mikellides, I. G., Brophy, J. R., Tighe, W. G., and Chien, K.-r., "Evaluation of 25-cm XIPSÂľ Thruster Life for Deep Space Mission Applications," 31st International Electric Propulsion Conference, Ann Arbor, Michigan, 2009, pp. 1–13.

[19]Corey, R. L. and Pidgeon, D. J., "Electric Propulsion at Space Systems/Loral," 31st International Electric Propulsion Conference, Ann Arbor, Michigan, 2009, pp. 1–17.

[20]Lieberman, M. A. and Lichtenberg, A. J., Principles of plasma discharges and materials processing, John Wiley and Sons, April 1994.

[21]Jain, S. K., Jain, A., and Hannurkar, P. R., "Indigenous development of a low cost high power 2 kW (CW), 2 . 45 GHz microwave system," Indian Journal of Pure & Applied Physics, Vol. 42, No. December, 2004, pp. 896–901.

[22]Windes, D., Dutkowski, J., Kaiser, R., and Justice, R., "Triservice-NASA cathode life test facility," Applied Surface Science, Vol. 146, 1999, pp. 75–78.

[23]Goebel, D. M. and Watkins, R. M., "Compact Lanthanum Hexaboride Hollow Cathode," Review of Scientific Instruments, Vol. 81, No. 8, Aug. 2010, pp. 083504.

[24]Jameson, K. K., Goebel, D. M., Hofer, R. R., and Watkins, R. M., "Cathode Coupling in Hall Thrusters," 30th International Electric Propulsion Conference, Florence, Italy, 2007, pp. 1–20.

[25]Florenz, R., Gallimore, A. D., and Peterson, P. Y., "Developmental Status of a 100-kW Class Laboratory Nested Channel Hall Thruster," 32nd International Electric Propulsion Conference, Wiesbaden, Germany, 2011, pp. 1–9.

[26]Goebel, D. M., Jameson, K. K., Katz, I., and Mikellides, I. G., "Potential Fluctuations and Energetic Ion Production in Hollow Cathode Discharges," Physics of Plasmas, Vol. 14, No. 10, 2007, pp. 103508.

[27]Goebel, D. M., Jameson, K. K., Katz, I., and Mikellides, I. G., "Plasma Potential Behavior and Plume Mode Transitions in Hollow Cathode Discharges," 30th International Electric Propulsion Conference, Florence, Italy, 2007, pp. 1–9.

[28]Mikellides, I. G. and Katz, I., "Wear Mechanisms in Electron Sources for Ion Propulsion, 1: Neutralizer Hollow Cathode," Journal of Propulsion and Power, Vol. 24, No. 4, July 2008, pp. 855–865.

[29]Goebel, D. M., Mikellides, I. G., Polk, J. E., Young, J., Tighe, W. G., and Chien, K.-r., "Keeper Wear Mechanisms in the XIPS 25-cm Neutralizer Cathode Assembly," 31st International Electric Propulsion Conference, Ann Arbor, Michigan, 2009, pp. 1–11.

[30]Mikellides, I. G., Goebel, D. M., Snyder, J. S., Katz, I., and Herman, D. a., "The discharge plasma in ion engine neutralizers: Numerical simulations and comparisons with laboratory data," Journal of Applied Physics, Vol. 108, No. 11, 2010, pp. 113308.

[31]Lisovski, V. A., "Criterion for microwave breakdown of gases," Technical Physics, Vol. 44, No. 11, 1999.

[32]Biswas, J. and Mitra, V., "High Frequency Breakdown and Paschen Law," Applied Physics, Vol. 381, 1979, pp. 377–381.

[33]Polk, J. E., Mikellides, I. G., Katz, I., and Capece, A. M., "Tungsten and Barium Transport in the Internal Plasma of Hollow Cathodes," Journal of Applied Physics, Vol. 105, No. 11, 2009, pp. 113301.

[34]Polk, J. E., Capece, A. M., Mikellides, I. G., and Katz, I., "Barium Depletion in the NSTAR Discharge Cathode After 30,472 Hours of Operation," 46th Joint Propulsion Conference, Nashville, TN, 2010.

[35]COMSOL, COMSOL Multiphysics RF Module User's Guide, 2007.